

# Proton-CAT: a Novel Proposal for Enhanced Proton Therapy

Zhao Sun,<sup>1</sup> Zhencen He,<sup>2,1</sup> Zhuohang He,<sup>1</sup> Junxiang Wu,<sup>1,3</sup> Liyuan Deng,<sup>1</sup>  
Ziqi Chen,<sup>1</sup> Junkang Jiang,<sup>1</sup> Hang Zhu,<sup>1</sup> Shuyu Zhang,<sup>2</sup> and Zhimin Hu<sup>1,\*</sup>

<sup>1</sup>Key Laboratory of Radiation Physics and Technology of Ministry of Education,  
Institute of Nuclear Science and Technology, Sichuan University, Chengdu 610064, China

<sup>2</sup>West China School of Basic Medical Sciences and Forensic Medicine, Sichuan University, Chengdu 610041, China

<sup>3</sup>Radiation Oncology Department Sichuan Cancer Hospital and Institute,  
Affiliated Cancer Hospital of University of Electronic Science and Technology of China, Chengdu 610041, China  
(Dated: March 15, 2024)

We propose an innovative nitrogen-targeted proton carbon alpha therapy method, abbreviated as Proton-CAT, which partially converts protons into carbon-12 and alpha particles through nuclear reactions between protons and nitrogen-15. The effectiveness of Proton-CAT was validated using Monte Carlo simulations, and the study focused on the relative energy deposition distribution. The findings indicate that the presence of nitrogen enhances the maximum dose level of protons, resulting in more severe damage confined to tumor cells. Statistical analysis of secondary ions demonstrated that Proton-CAT significantly increases the efficiency of carbon-12 and alpha particle production. Furthermore, our results revealed that elevating the nitrogen concentration significantly boosts the dose of carbon and alpha particles within the tumor region. These outcomes offer a novel pathway for proton radiation therapy and hold promise for contributing to the future development of proton therapy.

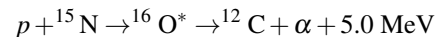
In this century, cancer will become the leading cause of premature death globally and the greatest obstacle to further increasing life expectancy [1]. Radiation therapy is an effective clinical treatment for malignant tumors. Currently, most clinical radiation therapy uses photon beams (e.g. X- and  $\gamma$ -rays) or electron beams with energies ranging from several to tens of MeV [2, 3]. If the dose is high enough, any radiation beam can destroy any cancer cell or living organism. Considering the physical properties of photons, normal tissues around the target volume still receive a large and unnecessary dose of radiation. However, the key factor in the development of radiation medicine has been how to avoid irradiating normal tissue [4].

For many years in parallel, proton and heavy ion radiation therapy has been developing tempestuously [5–8]. They take advantage of the physical properties of protons and heavy ions passing through matter to form Bragg peaks. When protons and heavy ions slow down by transferring momentum, the stopping power near the Bragg peak velocity significantly increases [9]. Therefore, the dose distribution of proton and heavy ion radiotherapy is better than that of photon radiotherapy. By adjusting the high-dose zone embedded in the tumor, it is expected to help increase tumor dose and reduce damage to normal tissue. The interaction of ionizing radiation from protons and heavy ions with tissues and organs can lead to local energy deposits large enough to trigger strand breaks in DNA, leading to mutations, chromosomal aberrations, and cell death [10]. However, protons mainly indirectly kill cells by causing single-strand breaks (SSBs). Cancer cells can only be killed if the next SSB can cut another strand off before the damaged DNA recovers, otherwise it will be repaired [11, 12]. This makes it difficult for protons to effectively treat chemoresistant and hypoxic tumors [12]. For

this reason, researchers widely regard carbon ions as the optimal heavy ions for therapeutic purposes. Not only do carbon ions have similar Bragg peak physical properties to protons, they also have higher linear energy transfer (LET) and unit energy deposition density than protons. This means that its relative biological effectiveness (RBE) at the Bragg peak is 2 to 3 times higher than that of protons [7, 8]. In other words, it possesses the ability to directly kill tumor cells by inducing double-strand breaks (DSBs), making the damaged cells more difficult to repair [11, 13]. Furthermore, due to the hypoxic nature of cancer cells, carbon exhibits a lower oxygen enhancement ratio (OER, the ratio of radiation doses required to cause the same damage in hypoxic and oxygenated cells) compared to protons [14, 15]. Higher RBE and lower OER values are characteristic biological advantages of carbon-ion with high LET. However, carbon ion therapy demands higher requirements for equipment and technology, making it more expensive compared to proton therapy, which also restricts its widespread clinical adoption and application scope [16].

In this Letter, we introduce an innovative approach to proton therapy, termed Nitrogen-Targeted Proton-Carbon-Alpha Therapy (Proton-CAT), leveraging the advantages of protons and carbon ions. Monte Carlo simulation results indicated that it contribute to an enhanced therapeutic effect through additional dose deposition of carbon ( $^{12}\text{C}$ ) and alpha. This novel method not only harnesses the inherent benefits of proton therapy but also amplifies its efficacy by incorporating the therapeutic potential of  $^{12}\text{C}$  and  $\alpha$ , offering a promising avenue for advanced cancer treatment strategies.

The conceptual diagram of Proton-CAT is shown in Fig. 1, it based on the proton and stable nitrogen isotope ( $^{15}\text{N}$ ) fusion reaction (PNFR) to convert protons into  $^{12}\text{C}$  and  $\alpha$ :



It based on nuclear reaction with a high cross-section when the proton energy ranges from 3 to 11 MeV, which produced a large number of secondary particles and releasing a large

\* huzhimin@scu.edu.cn

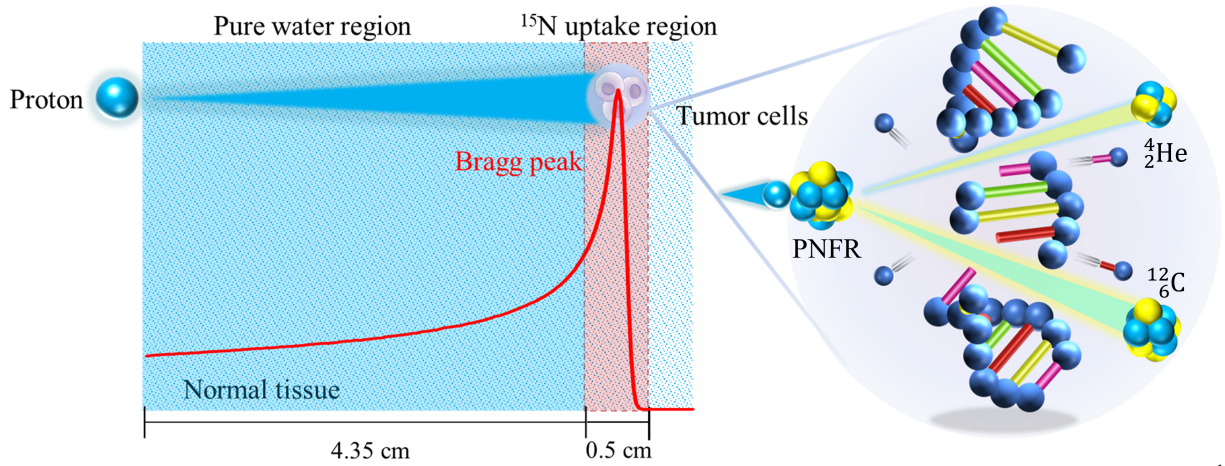


FIG. 1. Conceptual diagram of Proton-CAT and principles of geometric construction in Monte Carlo simulations. In the simulation,  $^{15}\text{N}$ -rich tumor phantom of 0.5 cm thickness covered the Bragg peak of the proton beams, and the tissue thickness in front of the tumor target was 4.35 cm.

amount of energy [17–19]. Simultaneously, the interaction between protons and  $^{15}\text{N}$  leads to the fragmentation of the excited oxygen ( $^{16}\text{O}$ ) into  $^{12}\text{C}$  and  $\alpha$ . As shown in Fig. 1, specialized tumor-specific drugs enriched with  $^{15}\text{N}$  dose-enhancement agent (DEA) are administered to the tumor region in practical therapy. When irradiated with the external proton beam, part of the protons is converted into  $^{12}\text{C}$  and  $\alpha$  particles via Proton-CAT in  $^{15}\text{N}$ -uptake region. These secondary short-range radiation sources are expected to cause more DSBs to the DNA of tumor cells, while minimizing cellular damage to normal tissues. Finally, proton therapy has acquired the advantages of heavy ion therapy. This approach, where each absorbed unit of energy causes additional damage to tumor cells, holds the potential to fundamentally enhance the efficiency of radiation therapy [20, 21]. In clinical settings, tumor cells e.g. gastric, colorectal, and breast cancers have higher uptake of glutamine ( $\text{C}_5\text{H}_{10}\text{N}_2\text{O}_3$ ) than normal cells [22]. Therefore,  $^{15}\text{N}$ -labeled glutamine can be applied to Proton-CAT as DEA. Compared to normal cells, if DEA uptake in the tumor was high enough then curing effect is achieved. This provides the possibility for clinical application of our method.

Herein, the aim was to verify the theoretical validity of the Proton-CAT. We further investigated the potential benefits of enhancing  $^{15}\text{N}$  concentration in Proton-CAT for proton therapy. Additionally, the secondary particles produced by Proton-CAT was calculated, aiming to quantify the contribution of each nuclear reaction to secondary particles and assess whether they could achieve a synergistic effect for dose enhancement.

The Geant 4 toolkit is used for simulation calculation, which is an open-source Monte Carlo simulation program widely used in medical physics [23]. In the current work, the physical list employed for all simulations is G4HadronPhysics QGSP\_BIC\_AllHP. It employs the binary cascade de-excitation model, electromagnetic physics option 4 as the standard, and a precision data-driven model for low-energy protons, neutrons, deuterium, tritium,  $^3\text{He}$ , and alpha particles. An assessment of both the binary cascade and standard electromagnetic physics option4 has been con-

TABLE I. Compositions, mass density and elemental proportion of the three-group tumor phantom.

Groups	Mass density ( $\text{g}/\text{cm}^3$ )	$^1_1\text{H}$	$^{16}_8\text{O}$	$^{15}_7\text{N}$
Pure water	1.000	66.7	33.3	0.0
with 10% $^{15}\text{N}$	1.139	60.0	30.0	10.0
with 30% $^{15}\text{N}$	1.538	46.7	23.3	30.0

ducted to ensure optimal agreement between simulated results and measurements in proton therapy [24]. In addition, it is created with the High-Precision Charged Particle physics model, which is suitable for energy below 200 MeV. The range threshold for all secondary particles production was set to 0.1 mm, below which the projectile trajectory is terminated and all remaining kinetic energy is deposited locally.

In the simulation, the geometry consists of two parts: water and tumor phantom. As shown in the blue zone in Fig. 1, considering that tissue is mainly composed of water, the material representing normal tissue in the simulation geometric model is defined as pure water. In order to reflect the dose enhancement brought about by Proton-CAT, the material within the tumor phantom is defined as a mixture of water and varying concentrations of  $^{15}\text{N}$  (red zone in Fig. 1). As shown in Table I, there were three uptake setups for the tumor region, namely, pure water ( $\text{H}_2\text{O}$ ), with 10%  $^{15}\text{N}$  (90% water + 10%  $^{15}\text{N}$ ) and with 30%  $^{15}\text{N}$  (70% water + 30%  $^{15}\text{N}$ ). Both the phantom and tumor are defined as cubes with width of 5 cm. A proton beam with assigned energy is directed from the front of the water, covering the entire target volume. Therefore, the thickness of water and tumor models was set to 4.35 cm and 0.5 cm, respectively, at 75 MeV incident energy to ensure coverage of the entire Bragg peak over the tumor region and the center of the tumor region corresponds to the point of maximum dose delivery for each proton. In our work, for each simulation run,  $10^9$  protons were transported through the target volume.

Fig. 2 show the percentage dose depth (PDD) in target volume of proton. The PDD in the pure water was used as the

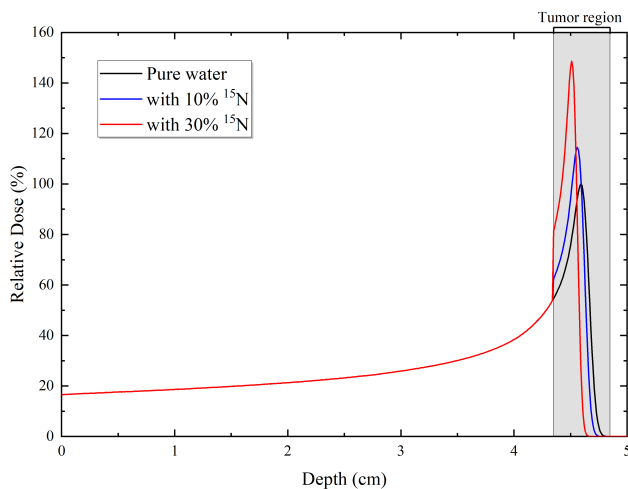


FIG. 2. The PDD of 75 MeV protons for three different materials: the black line represents the normalized PDD from the water phantom without  $^{15}\text{N}$  doping, while the blue and red lines represent the PDD compared to the water phantom when the maximum dose point of protons is located within the tumor region.

reference. The PDD increases with depth and reaches a Bragg peak near the maximum range. Compared to pure water, the doping of  $^{15}\text{N}$  can enhance the dose in the tumor volume and cause a forward shift of the Bragg peak. Due to protons release their last few MeV of kinetic energy upon reaching tumor region (the energy range with the largest nuclear reaction cross section), it lead to an increase selectivity of the Proton-CAT [25]. The secondary particles produced from the nuclear reaction between protons and  $^{15}\text{N}$  are responsible for a significant portion of dose delivery, and they deposit energy primarily through ionization processes. These deliveries and become more considerable as the concentration of  $^{15}\text{N}$  increases to 30%. In addition, from the Fig. 2, it can be observed that the accumulation of range straggling tends to broaden the peak with increasing depth. Nonetheless, the monoenergetic proton beam has a finite range and the deposited energy is un-homenergetic in tumor volume. Moreover, this finite range becomes more constrained with variations in the doping concentration within the tumor region.

This study exploits the nuclear reactions between protons and targeting elements to enhance the dose through the production of heavy secondary particles. We counted the secondary particles (mainly  $\alpha$  and  $^{12}\text{C}$ ) produced in the tumor region, are shown in Fig. 3. It can be seen that compared with the case of pure water, i.e., normal tissue, introducing  $^{15}\text{N}$  into the tumor area will produce more  $\alpha$  and  $^{12}\text{C}$  particles. The gain becomes more pronounced as the  $^{15}\text{N}$  concentration increases i.e., a threefold increase in  $^{15}\text{N}$  concentration results in more than a threefold increase in product particles. As mentioned before, these energetic secondary particles not only contribute to dose enhancement but also, compared to protons,  $\alpha$  and  $^{12}\text{C}$  particles with higher LET values can result in greater RBE. However, for normal tissue (i.e., without  $^{15}\text{N}$ ),  $\alpha$  and  $^{12}\text{C}$  particles will still be produced, attributed to nuclear reactions induced by the interaction between protons and  $^{16}\text{O}$ . The primary reactions generating  $\alpha$  and  $^{12}\text{C}$  parti-

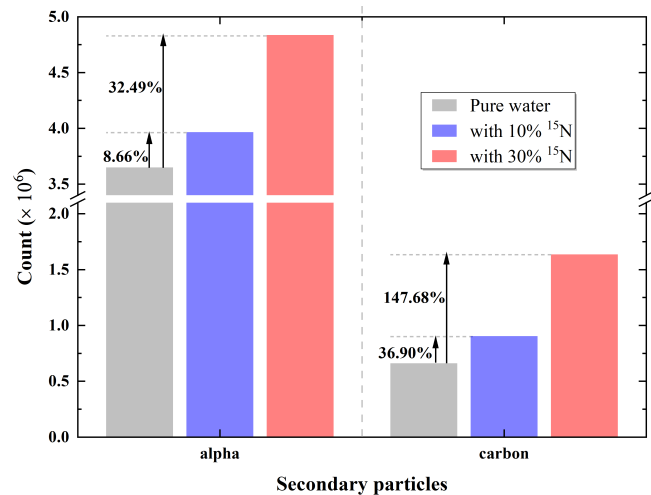


FIG. 3. The count of secondary particles generated by protons in the tumor region compared to a pure water phantom, as well as the gain relative to normal tissue.

cles in pure water are the  $^{16}\text{O}(p, \alpha)^{13}\text{N}$  and  $^{16}\text{O}(p, p'\alpha)^{12}\text{C}$  nuclear reactions, with relatively low thresholds of 5.66 and 7.16 MeV respectively [26–28]. It should be pointed out that for tumors containing 10% and 30% concentrations of  $^{15}\text{N}$ , the interaction of protons with  $^{16}\text{O}$  in water is another significant mechanism for generating alpha particles. Therefore, the number of  $\alpha$  produced in the tumor area is greater than that of  $^{12}\text{C}$ . Moreover, with the introduction of  $^{15}\text{N}$ , the  $^{12}\text{C}$  gain percentage is much greater than  $\alpha$ .

As shown in Fig. 4, we have made piecewise statistics on the energy of  $\alpha$  and  $^{12}\text{C}$  particles produced from tumor region. From Fig. 4(a),  $\alpha$  was mainly produced at 0–6 MeV. However, the  $\alpha$  produced by the nuclear reaction between protons and  $^{16}\text{O}$  cannot be ignored, the number of  $\alpha$  across increased significantly in all energy ranges. There are some important differences between  $\alpha$  and  $^{12}\text{C}$ . In pure water, the energy of the  $^{12}\text{C}$  produced was evenly distributed. However, we can see that the  $^{12}\text{C}$  produced by the Proton-CAT process was mainly distributed in 0–6 MeV. In addition, the increase in  $^{15}\text{N}$  concentration leads to a significant increase in  $^{12}\text{C}$ , especially in the energy range of 2–4 MeV. Accordingly, these additional product particles can result in a greater dose deposition within the tumor region.

From the results above, we can see that Proton-CAT can increase in deposited energy in the tumor region. The therapeutic effect was caused by both primary and secondary particles. As shown in Fig. 2, Proton-CAT generated a large number of secondary particles, which contributed to the total absorbed dose. In detail, the velocity of  $\alpha$  and  $^{12}\text{C}$  ions gradually slowed down and the LET increased at the cellular level after PNFR occurred. Their dose deposition contributes to the RBE of proton beam in the tumour region at the same time as the formation of the new Bragg peak [12]. Therefore, we have calculated the dose increase caused by secondary particles within the tumor region, as shown in Fig. 5. It can be observed that when 75 MeV protons were implanted, the absorbed dose of secondary particles produced by and PNFR increases significantly compared to pure water. The dose pro-

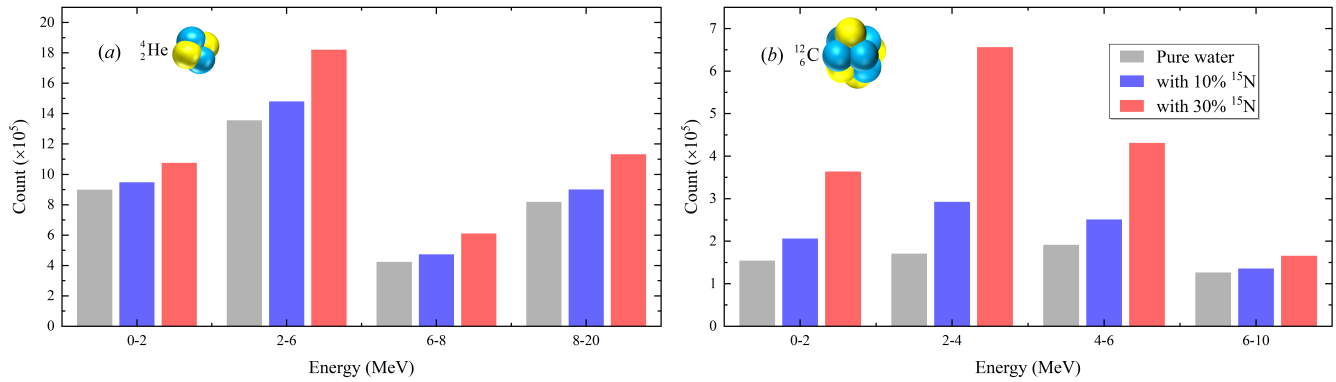


FIG. 4. Piecewise statistical results of (a)  ${}^{12}\text{C}$  and (b)  $\alpha$  particle energy generated in tumor region after  $10^9$  protons are implanted.

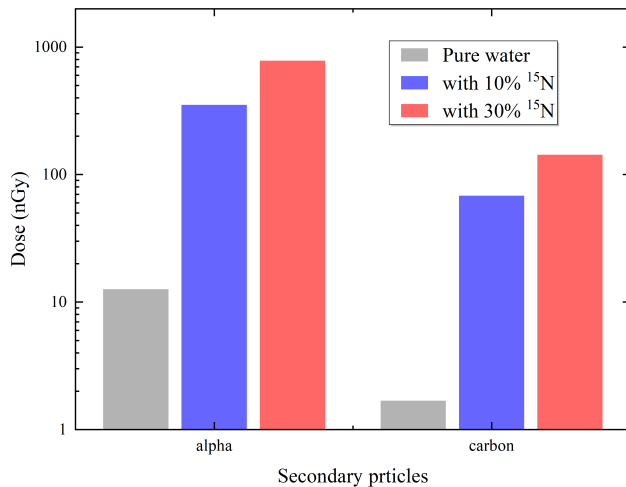


FIG. 5. The absorbed dose generated by proton-induced secondary particles ( $\alpha$  and  ${}^{12}\text{C}$ ) in the tumor region.

duced by secondary particles was much higher than that delivered without adding  ${}^{15}\text{N}$ . Analogously, Proton-CAT has an expected absorbed dose that overflows with the increase of  ${}^{15}\text{N}$  concentration. As shown in Fig. 4(b), Proton-CAT can generate numerous  ${}^{12}\text{C}$  with 0–6 MeV, further enhancing the dose within the tumor region. This is the greatest advantage of Proton-CAT. In fact, the total absorbed dose deposition of secondary particles can be highly dependent on the circum-

stances, including the incident proton energy, the geometric size of the tumor and the concentration of  ${}^{15}\text{N}$ .

In the present work, a novel enhanced proton treatment approach Proton-CAT based on the nuclear reaction between protons and  ${}^{15}\text{N}$  was proposed. Monte Carlo simulations were employed to evaluate the performance of Proton-CAT in proton therapy. In addition, varying concentrations of  ${}^{15}\text{N}$  were set to contrast the impact of concentration enhancement on dose deposition and the generation of secondary particles. To quantitatively assess the efficacy of secondary particles dose deposition in various scenarios, their average dose in the tumor region was determined. These results indicated that Proton-CAT demonstrates a dose enhancement advantage in proton therapy, with secondary particle  ${}^{12}\text{C}$  playing a crucial role therein. It must be emphasized that, despite our results confirming the fundamental effectiveness and advantages, further validation is required for the clinical application of this method. In future research, in vitro experiments will be conducted building upon the current simulation calculations, serving as the next step for the clinical application of Proton-CAT.

This work was supported by the National Natural Science Foundation of China (Nos. 12374234 and 12074352), the Sichuan Science and Technology Program (Grant No. 2023ZYD0017), the Defense Industrial Technology Development Program (Grant No. JCKYS2023212808) and the Fundamental Research Funds for the Central Universities in China (Grant No. YJ202144).

- [1] I. Soerjomataram and F. Bray, Planning for tomorrow: global cancer incidence and the role of prevention 2020–2070, *Nature reviews Clinical oncology* **18**, 663 (2021).
- [2] J. M. Park, J.-i. Kim, C. Heon Choi, E. K. Chie, I. H. Kim, and S.-J. Ye, Photon energy-modulated radiotherapy: Monte carlo simulation and treatment planning study, *Medical Physics* **39**, 1265 (2012).
- [3] K. R. Hogstrom and P. R. Almond, Review of electron beam therapy physics, *Physics in Medicine & Biology* **51**, R455 (2006).
- [4] W. Dörr and J. H. Hendry, Consequential late effects in normal tissues, *Radiotherapy and oncology* **61**, 223 (2001).
- [5] M. Durante, R. Orecchia, and J. S. Loeffler, Charged-particle therapy in cancer: clinical uses and future perspectives, *Nature Reviews Clinical Oncology* **14**, 483 (2017).
- [6] A. Bhogale, S. Bhattacharjee, M. R. Chowdhury, C. Bagdia, M. Rojas, J. Monti, A. Jorge, M. Horbatsch, T. Kirchner, R. Rivarola, *et al.*, Electron emission from water vapor under the impact of 250-keV protons, *Physical Review A* **105**, 062822 (2022).

- [7] T. Liamsuwan, M. Hultqvist, L. Lindborg, S. Uehara, and H. Nikjoo, Microdosimetry of proton and carbon ions, *Medical Physics* **41**, 081721 (2014).
- [8] M. C. Frese, K. Y. Victor, R. D. Stewart, and D. J. Carlson, A mechanism-based approach to predict the relative biological effectiveness of protons and carbon ions in radiation therapy, *International Journal of Radiation Oncology\* Biology\* Physics* **83**, 442 (2012).
- [9] C. Shepard, D. C. Yost, and Y. Kanai, Electronic excitation response of dna to high-energy proton radiation in water, *Physical Review Letters* **130**, 118401 (2023).
- [10] E. J. Moding, M. B. Kastan, and D. G. Kirsch, Strategies for optimizing the response of cancer and normal tissues to radiation, *Nature reviews Drug discovery* **12**, 526 (2013).
- [11] M. Souici, T. T. Khalil, D. Muller, Q. Raffy, R. Barillon, A. Belafrites, C. Champion, and M. Fromm, Single-and double-strand breaks of dry dna exposed to protons at bragg-peak energies, *The Journal of Physical Chemistry B* **121**, 497 (2017).
- [12] D. Schardt, T. Elsässer, and D. Schulz-Ertner, Heavy-ion tumor therapy: Physical and radiobiological benefits, *Reviews of modern physics* **82**, 383 (2010).
- [13] A. V. Solov'yov, E. Surdutovich, E. Scifoni, I. Mishustin, and W. Greiner, Physics of ion beam cancer therapy: a multiscale approach, *Physical Review E* **79**, 011909 (2009).
- [14] H. Suit, T. DeLaney, S. Goldberg, H. Paganetti, B. Clasié, L. Gerweck, A. Niemierko, E. Hall, J. Flanz, J. Hallman, *et al.*, Proton vs carbon ion beams in the definitive radiation treatment of cancer patients, *Radiotherapy and Oncology* **95**, 3 (2010).
- [15] T. Wenzl and J. J. Wilkens, Modelling of the oxygen enhancement ratio for ion beam radiation therapy, *Physics in medicine & biology* **56**, 3251 (2011).
- [16] M. d. Nunes, *Protontherapy versus carbon ion therapy: advantages, disadvantages and similarities* (Springer, 2015).
- [17] A. Schardt, W. A. Fowler, and C. C. Lauritsen, The disintegration of  $^{15}\text{N}$  by protons, *Physical Review* **86**, 527 (1952).
- [18] S. Bashkin, R. Carlson, and R. Douglas, Cross sections for elastic scattering and reactions due to protons on  $\text{N}^{15}$ , *Physical Review* **114**, 1543 (1959).
- [19] A. Nurmukhanbetova, V. Goldberg, D. Nauruzbayev, G. Rogachev, M. Golovkov, N. Mynbayev, S. Artemov, A. Karakhodjaev, K. Kuterbekov, A. Rakhymzhanov, *et al.*, Implementation of ttik method and time of flight for resonance reaction studies at heavy ion accelerator DC – 60, *Nuclear Instruments and Methods in Physics Research Section A: Accelerators, Spectrometers, Detectors and Associated Equipment* **847**, 125 (2017).
- [20] A. A. Lipengolts, Y. A. Finogenova, V. A. Skribitsky, and E. Y. Grigorieva, Binary technologies of malignant tumors radiotherapy, *Journal of Physics: Conference Series* **2058**, 012039 (2021).
- [21] Heavy charged particles: Does improved precision and higher biological effectiveness translate to better outcome in patients?, *Seminars in Radiation Oncology* **28**, 160 (2018).
- [22] B. I. Reinfeld, M. Z. Madden, M. M. Wolf, A. Chytil, J. E. Bader, A. R. Patterson, A. Sugiura, A. S. Cohen, A. Ali, B. T. Do, *et al.*, Cell-programmed nutrient partitioning in the tumour microenvironment, *Nature* **593**, 282 (2021).
- [23] S. Agostinelli, J. Allison, K. a. Amako, J. Apostolakis, H. Araujo, P. Arce, M. Asai, D. Axen, S. Banerjee, G. Barrand, *et al.*, Geant4—a simulation toolkit, *Nuclear instruments and methods in physics research section A: Accelerators, Spectrometers, Detectors and Associated Equipment* **506**, 250 (2003).
- [24] C. Z. Jarlskog and H. Paganetti, Physics settings for using the geant4 toolkit in proton therapy, *IEEE Transactions on nuclear science* **55**, 1018 (2008).
- [25] A. Mazzone, P. Finocchiaro, S. L. Meo, and N. Colonna, On the (un) effectiveness of proton boron capture in proton therapy, *The European Physical Journal Plus* **134**, 361 (2019).
- [26] J. Cho, K. Grogg, C. H. Min, X. Zhu, H. Paganetti, H. C. Lee, and G. El Fakhri, Feasibility study of using fall-off gradients of early and late pet scans for proton range verification, *Medical physics* **44**, 1734 (2017).
- [27] R. Chapman and A. Macleod, Proton nuclear reaction cross sections in oxygen and neon at 13 mev, *Nuclear Physics A* **94**, 313 (1967).
- [28] R. Chapman and A. MacLeod, The mechanism of the  $^{16}\text{O}(p, p'\alpha)^{12}\text{C}$  and  $^{12}\text{Ne}(p, p'\alpha)^{16}\text{O}$  reactions at 13 mev, *Nuclear Physics A* **94**, 324 (1967).